

Ti/TiN/HA coating on Ti–6Al–4V for biomedical applications

E. Mohseni^a, E. Zalnezhad^{b,*}, A.R. Bushroa^{a,*}, Abdel Magid Hamouda^c, B.T. Goh^d, G.H. Yoon^e

^aCenter of Advanced Manufacturing and Material Processing, Department of Engineering, Faculty of Engineering, University of Malaya, 50603, Malaysia

^bDepartment of Mechanical Engineering, Hanyang University, 222 Wangsimni-ro, Seongdong-gu, Seoul 133-791, Republic of Korea

^cMechanical and Industrial Engineering Department, College of Engineering, Qatar University, P.O. Box 2713, Doha, Qatar

^dLow Dimensional Materials Research Centre, Department of Physics, Faculty of Science, University of Malaya, 50603 Kuala Lumpur, Malaysia

^eSchool of Mechanical Engineering, Hanyang University, Seoul, Republic of Korea

Received 22 May 2015; received in revised form 29 June 2015; accepted 14 July 2015

Available online 21 July 2015

Abstract

An unbalanced physical vapor deposition (PVD) magnetron sputtering technique was used to deposit a titanium/titanium nitride/hydroxyapatite (Ti/TiN/HA) multilayer coating on Ti–6Al–4V. The Taguchi optimization method with an orthogonal array of L9 was utilized to determine the optimal conditions of coating for better surface integrity. The effects of the temperature, DC bias voltage, nitrogen flow rate, and DC power on the adhesion strength, coefficient of friction, surface hardness, and surface roughness were investigated. In achieving the optimized coating parameters, the signal to noise (S/N) response analysis method was implemented. Confirmation tests were carried out to demonstrate the improvement using the best combination of parameters obtained from the optimization process. The surface hardness of the Ti/TiN coated and uncoated specimens was enhanced by 14% and 48%, respectively. The adhesion strength of the coating to the substrate, coefficient of friction, and surface roughness were improved by 5.1%, 43%, and 10.52%, respectively. Finally, hydroxyapatite was successfully deposited atop Ti/TiN coated Ti–6Al–4V using a PVD sputtering technique to improve the biocompatibility of the substrate. The presence of Ti/TiN interfacial thin layers between the HA layer and substrate enhanced the adhesion strength of the HA coating on the substrate by 44.57% compared to the HA-coated substrate without the interfacial layers.

© 2015 Elsevier Ltd and Techna Group S.r.l. All rights reserved.

Keywords: Ti–6Al–4V; PVD magnetron sputtering; Ti/TiN coating; Hydroxyapatite; Mechanical properties

1. Introduction

1.1. Titanium alloys for biomedical applications

Titanium (Ti) and its alloys (typically Ti–6Al–4V) are frequently used in surgical implants and total joint replacement applications (TJR) as a result of their high biocompatibility and mechanical properties. The high applicability of titanium alloys results from their low density, corrosion resistance, and low elastic modulus, which reduce stress shielding [1–4]. However, other surgical alloys have demonstrated better adhesive and

abrasive wear properties than titanium alloys [4–8]. Subjecting an orthopedic device to relative sliding at the Ti alloy/metal or Ti alloy/polyethylene interface results in fracture of the passivating surface oxide along with the creation of particulate metal and polyethylene debris and increased metal ion release. Accumulation of wear debris causes bone resorption, jeopardizing the long-term stability of the prosthesis [9,10].

Therefore, to improve the mechanical properties of Ti–6Al–4V, a variety of surface modifications have been utilized including nitrogen implantation and ultra-passivation of titanium [11]. These methods have become a standard procedure for Ti alloys. However, they are not guaranteed to provide adequate wear resistance of critical TJR components and long-term service due to the rapid thinning of the $\leq 0.5\ \mu\text{m}$ thick hardened layer [12,13]. The major constraints identified in the

*Corresponding author. Tel.: +82 2 2222 0442; fax: +82 2 2222 3406.

*Corresponding author.

E-mail address: erfan@hanyang.ac.kr (E. Zalnezhad).

mentioned alloy are related to the tribological behavior, mainly in dry sliding wear due to its relatively low surface hardness and significant ductility.

1.2. Hard tissue coating

The discipline of surface engineering allows improvement of bulk material properties by applying micro and nanocoatings. Currently, there is high demand for hard thin film coating materials such as titanium nitride (TiN) to enhance the mechanical properties of Ti alloys [14–17]. A TiN coating layer has been widely used to enhance the hardness of different materials. However, it is difficult to control the properties of the film such as the grain size, film thickness, and step coverage [18,19]. Moreover, only limited data has been published regarding the influence of the TiN coating layer on various parameters such as the scratch force, hardness, and roughness as well as the effect of the TiN coating layer microstructure of the deposited film [20,21]. Investigation of this coating will demonstrate the possibility of obtaining high strength, hardness, and simultaneously good decorative and protective surface properties [22]. Surface modifications have attracted more attention with new techniques such as high power laser and vacuum processing. This fact is interesting since these new techniques are highly comparable with traditional surface modification techniques ranging from painting and glazing to electroplating [23–24].

Based on a study by Mohseni et al. [25], titanium alloys such as Ti–6Al–4V and a TiN coating layer are commonly used metallic materials for medical implants in orthopedic and dental applications. However, there have been reports of inflammatory reactions around these implants as a result of the creation of an avascular fibrous tissue that encapsulated the implants. Thus, a hydroxyapatite layer coating can be deposited on the metal alloy to assist the osseointegration of these implants with surrounding tissues. Hydroxyapatite (HA: $\text{Ca}_{10}(\text{PO}_4)_6(\text{OH})_2$) is a pure calcium phosphate phase and a preferred biomaterial for both dental and orthopedics due to its favorable osteoconductive and bioactive properties [26].

Physical vapor deposition (PVD) is one of the most common vacuum coating processes which has the ability to deposit the film material atom by atom on a substrate. The low process temperature allows coating material to be deposited without reduction of the corrosion resistance, loss of hardness, or distortion compared to other deposition techniques conducted at higher temperatures. Sputtering, ion plating, and thermal evaporation are three main techniques for applying PVD coatings [27–29].

1.3. Magnetron sputtering PVD coating

Table 1 tabulates some of the vacuum coatings available to increase the tribological properties of the sliding system. The PVD magnetron sputter coating technique is an extremely flexible coating technique that can be applied to coat virtually any material [30–32].

Good uniformity, better step coverage, strong adhesion of the coating to the substrate, and a small shadow effect are a few of the advantages of the sputtering technique. Good

Table 1

Thin film coatings for tribological and surface integrity applications.

Coating technique	Materials
Thermal evaporation	Au, Ag, MCrAlY's, Cr, Mo
Sputtering	SiO, SiO ₂ , Cr, Mo, Au, TiC, TiN, Al ₂ O ₃ , WS ₂ , MoS ₂ , Si ₃ N ₄
Ion plating	Cr, Mo, TiC, TiN, Au, Ag, Si ₃ N ₄

Table 2

Chemical composition of Ti–6Al–4V.

Chemical composition of Ti–6Al–4V Alloy (wt%)						
Al	V	Fe	C	O	N	Ti
6.2	4.1	0.22	0.01	0.122	0.012	Bal.

control of the effects of the parameters on the film characteristics including the film density, roughness, wear resistance, and adhesion strength is one important feature of the sputtering technique. Typical control parameters include the substrate temperature, process pressure, nitrogen flow rate, substrate bias voltage, and process DC power [28].

An optimization technique for the sputtering parameters is necessary to achieve the best surface integrity. In this sense, the Taguchi method, which is an experimental design technique, was used to dramatically decrease the number of experiments by using orthogonal arrays and minimizing the out of control factors [33–36].

In this work, optimization was performed to determine the influence of surface modification of a Ti/TiN multilayer coating on Ti–6Al–4V to optimize the effects of the temperature of the substrate, DC power, nitrogen flow rate, and DC bias voltage on the adhesion strength, surface hardness, and roughness of the coating. Moreover, confirmation tests were conducted to demonstrate the optimization. Finally, to increase the biocompatibility of the substrate, an HA thin film was deposited on the existing Ti/TiN layers.

2. Materials and methods

2.1. Substrates

Ti–6Al–4V was utilized in this study. The composition of the material characterized by EDX is given in Table 2. The Ti–6Al–4V samples were ground with 400 to 2000 SiC paper and mirror finished with polycrystalline diamond suspended liquid (Buehler). The substrates were cleaned by an ultrasonic machine using acetone for 20 min, followed by rinsing with distilled water and drying by nitrogen gas to prevent contamination.

2.2. Coating

A PVD magnetron sputtering machine (TF450 Sputtering System, SG Control Engineering, Singapore) was used for the

coating process on the Ti–6Al–4V substrate. The system includes 600 W RF and 1200 W DC generators with 4" × 12" electrodes. The distance between the target and sample was 150 mm. A 99.995% pure titanium target was used for the sputtering process. Before introducing the nitrogen gas for sputtering, the chamber was evacuated to below 2×10^{-5} Torr. During the experiment, a working pressure of 5.2×10^{-5} Torr was maintained. The effects of the coating parameters including the DC bias voltage, nitrogen flow rate, substrate temperature, and DC power on the surface roughness, hardness, adhesion strength, coefficient of friction, and microstructure of the sputtered TiN thin film were investigated. Subsequently, the hydroxyapatite thin layer was deposited on Ti/TiN layers by PVD magnetron sputtering at an RF power of 200 W, an argon flow rate of 15 sccm, and a temperature of 250 °C for a duration of 10 h. Before introducing argon gas for sputtering, the chamber was evacuated to below 2×10^{-6} Torr. A pressure of 3.2×10^{-3} Torr was maintained during the deposition process. Finally, the samples were heat-treated at 700 °C for 2 h to improve the adhesion strength between the thin film coatings and substrate.

2.3. Surface characterization

Elemental characterization of the hard thin film ceramic coatings was conducted by utilizing integrated energy dispersive X-ray spectroscopy with FESEM using (FE/SEM-FEG) and focused ion beam techniques (FEI Quanta FEG250). In addition, X-ray diffraction (XRD) analysis of the coating layers was performed by PANalytical Empyrean with a Cu K α wavelength, where its diffraction angle was set between 20° and 80° and the scanning speed was determined to 5°/min. The diffusion rate and chemical composition of the various coating layers accompanied by their attributed bulk substrate were investigated by an EDX cross-section line scanning technique (JEOL, JSM-7600F).

2.4. Surface mechanical properties

The hardness of the deposited layer was determined by a microhardness testing machine (HMV Micro Hardness Tester Shimadzu). The surface roughness of the TiN-coated samples was evaluated by a roughness tester machine (MAHR).

The adhesion strength and coefficient of friction of the coating were determined using microscratch test equipment (Micro Material Ltd., Wrexham, UK) with a 25 μ m (radius) diamond tip. Adhesion of the films to the substrates was quantitatively measured using a scratch test machine. A Rockwell type diamond indenter with a radius of 25 μ m was applied to the sample during the test with a sliding velocity of 5 μ m/s while increasing the load by 9.2 mN/s. The scratch length during the scratch test was 600 μ m.

In the scratch test, a critical load (L_C) was used to measure the adhesion strength of the coating to the substrate. In order to determine the magnitude of the critical load, an acoustic signal, friction curve, and microscope observation were employed. The acoustic signal provided by the film delamination was utilized to characterize the L_C . Acoustic emission (AE) is

defined as the elastic wave created by internally stored energy in the material structure being released. During the adhesion testing, the AE can be detected provided that the binding energy between the coating and the surface of the substrate is adequate. When a failure limit is reached, spontaneous shock wave bursts occur as a result of the formation and propagation of microcracks. Microcracks originate at surface notches, inside the coating or inside the substrate, where the local stresses exceed the fracture stress. It is imperative, as recognized by the scratch test operators, that when the L_C is reached, the succession of single shock wave bursts and the emitted signal spectrum will not be continuous. The shock wave propagation is affected by the sample geometry with respect to surface reflections which cause surface waves.

Analysis of the changes of the acoustic signal together with the friction force and microscopic observations of the topography of the scratch test tracks was used to determine the normal forces leading to cohesive and adhesive destruction of the coatings. The friction coefficient and acoustic emission signals were recorded. AE is constituted by elastic waves generated by the sudden crack in materials when an external load is applied. The penetration depth of the indenter as a function of the critical load was also analyzed [37].

3. Experimental design by the Taguchi optimization method

Traditional experimental design methods are very difficult and complex. The number of experiments increases dramatically as the number of coating parameters increases. Therefore, the factors causing variations should be specified and evaluated

Table 3
Parameters for depositing Ti/TiN coating.

Level	Parameters			
	A: DC power (W)	B: Temperature (°C)	C: Substrate bias voltage (V)	D: Nitrogen flow rate (%)
1	300	150	25	3
2	400	200	50	4
3	500	250	75	5

Table 4
The standard L9 orthogonal array and calculated S/N ratios value.

Experimental number	A	B	C	D	S/N ratio of microhardness	S/N ratio of Scratch force	S/N ratio of roughness
1	1	1	1	1	51.55	59.57	24.01
2	1	2	2	2	51.10	63.69	24.01
3	1	3	3	3	51.46	66.21	28.40
4	2	1	2	3	51.03	62.37	26.56
5	2	2	3	1	48.88	62.99	27.74
6	2	3	1	2	49.01	57.06	24.58
7	3	1	3	2	48.91	63.27	13.81
8	3	2	1	3	48.78	58.19	26.20
9	3	3	2	1	49.16	63.36	27.74

under laboratory conditions. Parameter design, of which the Taguchi method is the most reliable, is an engineering technique for process design which focuses on specifying the factor settings to produce the best levels of a quality characteristic (performance measure) with a minimum amount of variation [38]. To accommodate this requirement, the Taguchi method creates a standard orthogonal array. Instead of calculating the standard deviation, the signal-to-noise S/N ratio is used as a measurable value because as the mean increases, the standard deviation also increases and vice versa [39].

Taguchi empirically demonstrated that the two stage optimization procedure including S/N ratios yields a combination of parameter levels, where the standard deviation is minimized while keeping the mean on target [40]. This conveys the notion that engineering systems behave in such a way that the manipulated production factors can be classified into the following three categories.

1. Control factors which influence the process variability, as measured by the S/N ratio.
2. Signal factors which do not influence the process mean or S/N ratio.
3. Factors which do not affect the process mean or S/N ratio.

Practically, the mean value of the target is not fixed during the development of the process. Improvement of measurement and quality through minimizing the variables are two areas in which the concepts of the S/N ratio are useful. The characteristics of the S/N ratio for this study can be classified into three different categories: nominal is better, larger is better, and smaller is better. The last two categories can be used for the optimization in this study and the formulas are given by Eqs. (1) and (2), when the characteristic is continuous [41].

- Smaller is better characteristic,

$$S/N = -10 \log \frac{1}{n} \left(\sum y^2 \right) \quad (1)$$

- Larger is better characteristic,

$$S/N = -10 \log \frac{1}{n} \left(\sum \frac{1}{y^2} \right) \quad (2)$$

Here, n is the number of observations and y is the recorded data. In the Taguchi method, the optimum condition of coating required for the best surface roughness was obtained by Eq. (1), “the smaller the better” signal to noise ratio. The best adhesion and hardness values were attained using Eq. (2), “the larger the better” case using a MINITAB 14 Program. The coating parameter ranges and initial parameter values were chosen according to the device hand book and a Zalnezhad et al. [42] report. The coating parameters are shown in Table 3. For the nine experiments, the details of the combination of the experimental condition levels for each control factor (A–C)

and calculated S/N ratios for the roughness, adhesion, and hardness are shown in Table 4. The calculated S/N ratios will be discussed later.

4. Results and discussion

4.1. Coating morphology and elemental composition of the TiN layer

The cross-sectional view of the substrate along with the Ti/TiN coating is shown in Fig. 1. The coating structure was found to be compact and homogeneous, which can be due to

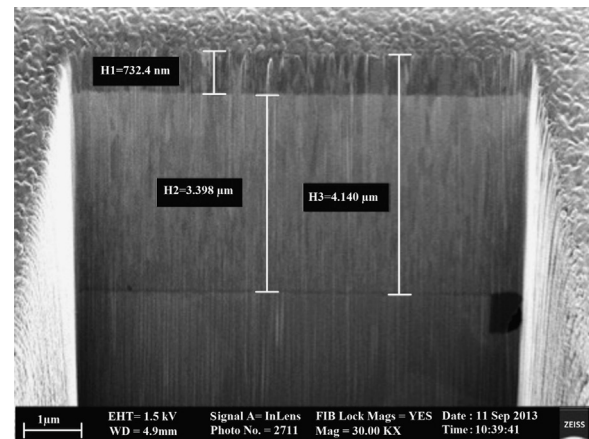


Fig. 1. The FIB-SESEM cross-sectional image of the Ti/TiN coated Ti-6Al-4V.

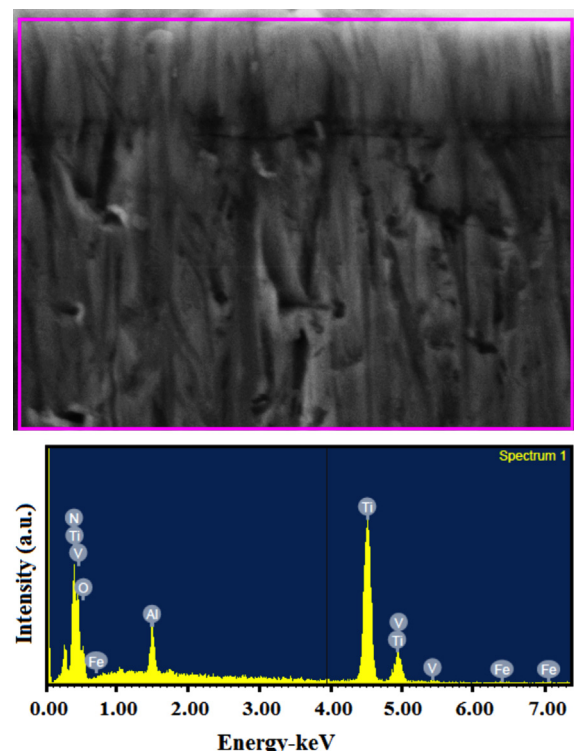


Fig. 2. EDX spectrum of the TiN Coating on Ti-6Al-4V.

dense nucleation of the depositing materials. In order to obtain an explicit view of the coating microstructure, the focused ion beam (FIB) technique was utilized. The FIB images show that the coating interlayer is perfectly bonded at the substrate–coating interface. As observed in Fig. 1, the upper TiN layer has a columnar structure. The results are in good agreement with a Dobrzański et al. [43] report.

Fig. 2 shows the chemical compositions of the various coating layers accompanied by their attributed bulk substrates obtained by an EDX cross-sectional line scanning technique. The qualitative EDX measurements prove the deposition of intended materials. The results of the XRD analysis in Fig. 3 show that the coatings contain a TiN type phase formed on the coated Ti–6Al–4V surface, as expected. Increasing DC power and DC bias voltage resulted in denser surfaces, as observed in Fig. 4. In Fig. 4c and b, it can be observed that coating with a higher DC bias voltage makes the surface denser compared to the low DC bias voltage.

4.2. Mechanical properties

The adhesion strength (scratch force), surface hardness, and roughness of the coated surface were measured three times and the average values are summarized in Table 5.

The friction curve, acoustic signal, and microscope observation were utilized in order to measure the magnitude of the critical load, L_c , which is the reference of the adhesion strength in the scratch test. The acoustic signal generated by delamination of the film can be used to characterize the critical load, L_c . The minimum load at which the first chipping occurs is termed the lower critical load, L_{c1} , while the loads corresponding to the delamination and total exposure of the coating are termed the critical load, L_{c2} , and L_{c3} , respectively [44]. Fig. 5(A and B) shows the results of the scratch adhesion test on a coated sample and the critical load accompanied by force and depth versus distance graphs. The weakest scratch force (coating adhesion) was achieved with a DC power of 300 W and a DC bias voltage of 25 V, while the strongest coating adhesion of 2112 mN was

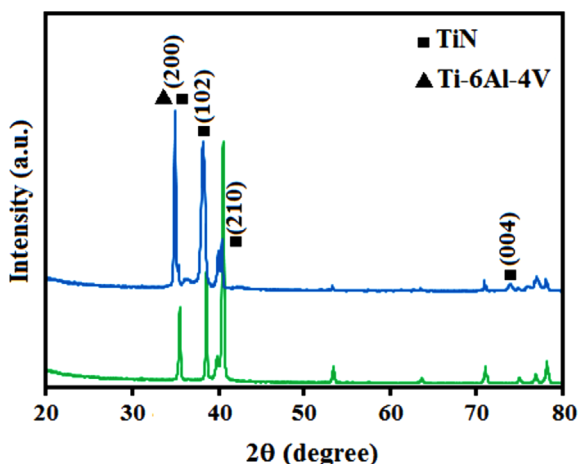


Fig. 3. XRD spectra of a TiN coating on the Ti–6Al–4V alloy and uncoated alloy.

obtained with a DC power of 300 W and a DC bias voltage of 75 V.

4.3. Coefficient of friction

The force required to detach the coating layer from the substrate is known as the scratch force (adhesion strength). Friction can be specified as the resistance tangential force to a relative motion between two surfaces in contact. Eq. (3) shows the formula for the friction force:

$$F = \mu \cdots N \quad (3)$$

where N is the normal force and μ is the coefficient of friction (COF) [45,46].

During the scratch adhesion test, based on Eq. (3), the coefficient of friction was calculated and plotted vs. the scratch length. The point that the indenter touches the substrate and penetrates into it is known as the total failure and is marked on the plot based on its corresponding failure load [47]. Fig. 6 illustrates the results of the calculated coefficient of friction versus distance for the (a) lowest adhesion, (b) highest adhesion, and (c) confirmation test. The graphs in (a) and (b) were drawn according to the data in Fig. 5 and the graph in (c) is based on the confirmation test after performing the optimization and achieving the best combination for adhesion, which will be explained later in this manuscript.

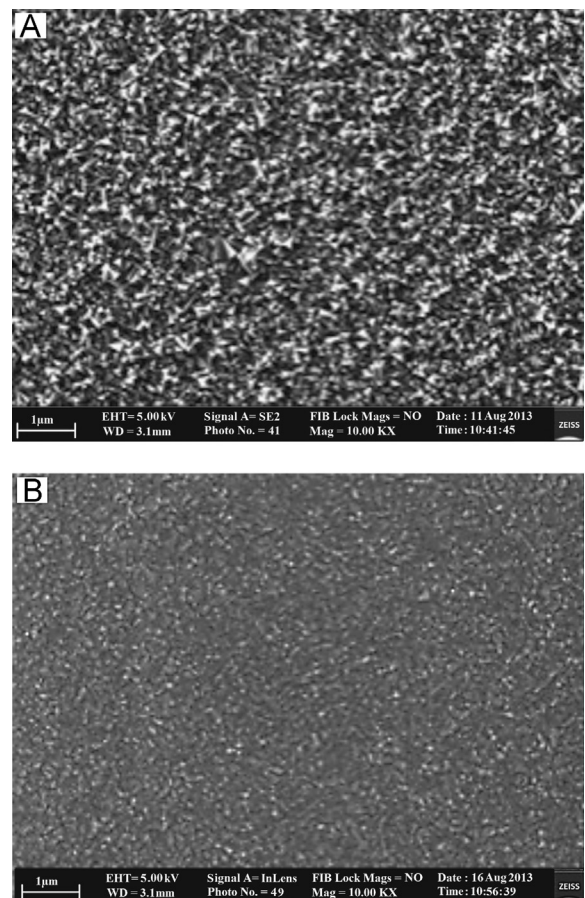


Fig. 4. Typical microstructure of TiN coating at different conditions (a) low substrate bias voltage (25 V), and (b) high substrate dc bias voltage (75 V).

Table 5
Experiment result.

Experiment	Measured surface hardness (HV)			Avg. microhardness (HV)			Measured scratch force (mN)			Avg. scratch force (mN)			Measured surface roughness (μm)			Avg. roughness (μm)	
	1st	2nd	3rd	1st	2nd	3rd	1st	2nd	3rd	1st	2nd	3rd	1st	2nd	3rd		
1	378	392	364	378			910	706	1240	952			0.048	0.065	0.082	0.063	
2	412	397	385	398			1530	1535	1525	1530			0.047	0.055	0.087	0.063	
3	376	378	368	374			1920	2112	2100	2044			0.027	0.035	0.052	0.038	
4	340	358	370	356			1253	1359	1330	1314			0.032	0.056	0.53	0.047	
5	292	266	276	278			1450	1359	1426	1411			0.033	0.025	0.065	0.041	
6	276	298	272	282			765	696	679	713			0.055	0.063	0.059	0.059	
7	269	274	294	279			1269	1500	1607	1458			0.188	0.201	0.223	0.204	
8	267	283	275	275			763	834	839	812			0.052	0.046	0.049	0.049	
9	281	293	287	287			1452	1432	1535	1473			0.038	0.047	0.038	0.041	

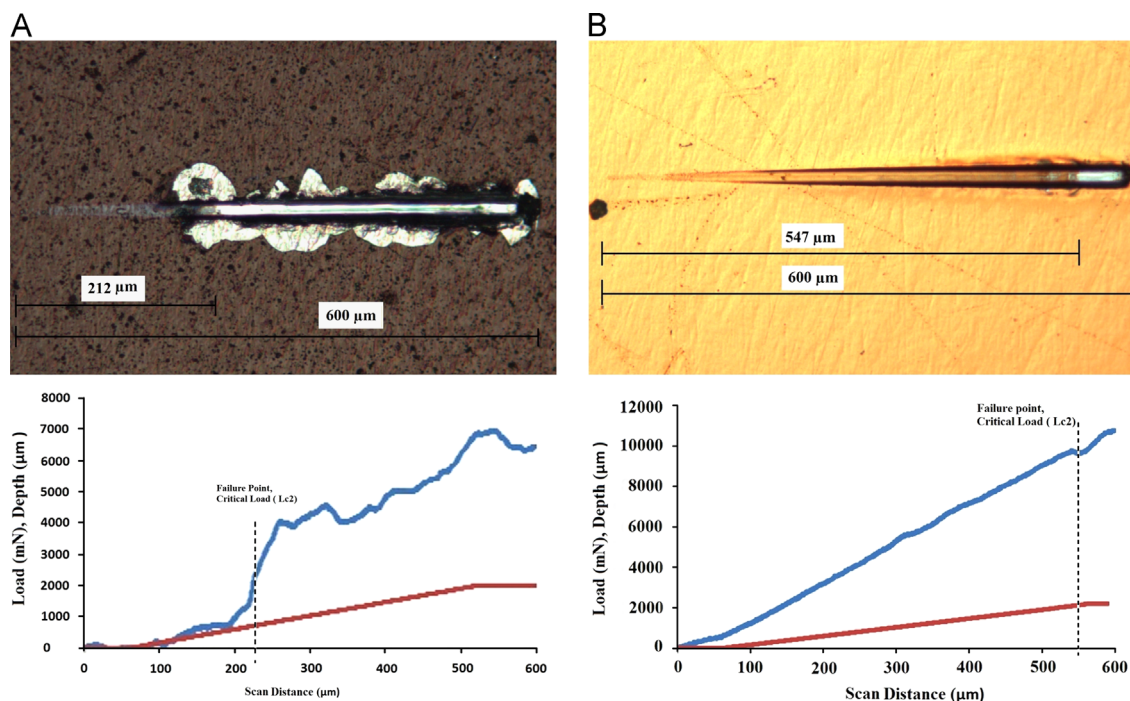


Fig. 5. Scratch adhesion testing on a coated sample and the critical load accompany with their force and depth versus distance graphs. (A) Weakest coating adhesion (scratch force), 706 mN, DC power (300 W), DC bias voltage (25 V) and (B) strongest coating adhesion, 2112 mN, DC power (300 W), DC bias voltage (75 V).

Based on the results of the scratch test, the lowest adhesion occurs at a distance of 212 μm from the starting point of the test. Hence, the calculated COF for the lowest adhesion based on Fig. 6(a) was 0.32. In the same way, the failure point of the coated substrate with the highest adhesion (Fig. 6(b)) occurs at a distance of 547 μm from the starting point. The coefficient of friction was 0.26.

4.4. Analyzing and evaluating the results using the Taguchi method

The signal to noise ratio is known as the most fundamental criterion in the Taguchi method to analyze experimental data. The predictable degree of a process or product in the presence

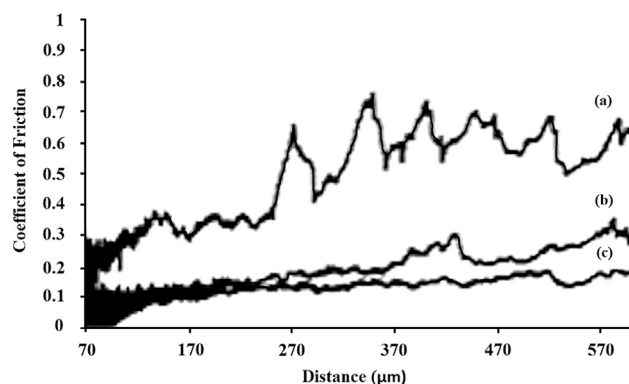


Fig. 6. Coefficient of friction for graph (a) (the lowest adhesion), graph (b) (the highest adhesion), and graph (c) (the confirmation test).

of noise factors can be determined from the S/N ratio. According to the Taguchi method, the S/N ratio in this study should have a minimum value for surface roughness and a maximum value for hardness and adhesion for better surface integrity. Table 4 shows the calculated S/N ratio for the surface roughness, hardness, and scratch force where Tables 5–7 show the S/N responses for each level of measured data, respectively. These data were also plotted and are shown in Fig. 7. Here, A_i is the average of all S/N ratios in Table 5 that has the same experimental level (i) under parameter A. In this case, (i) is equal to 1, 2, and 3, corresponding to the three parameter levels introduced in Table 3. Calculation of the S/N responses for B_i and C_i was carried out in the same way. According to the definition of the method, “the higher the better criteria” indicates that the highest S/N will reflect the best response, which results in the lowest noise effect in the results. In the current study, this criterion was used to define the optimal parameters for coating to obtain the highest surface hardness. Based on the higher S/N response, Fig. 7(A) illustrates the significance of the DC power (factor A), temperature (factor B), substrate DC bias voltage (factor C), and nitrogen flow rate (factor D) to obtain the best surface hardness. Moreover, the response values for the surface hardness, scratch force, and surface roughness were calculated and are tabulated in Tables 6–8, respectively.

The best parameters to obtain the highest value of the surface hardness are A_1 for the DC power parameter, B_1 for temperature, C_2 for the substrate bias voltage, and D_3 for the nitrogen flow rate. Therefore, $A_1B_1C_2D_3$ was the optimal combination to obtain the best surface hardness within the tested range. A confirmation test was carried out using this combination to validate the optimization results. In the confirmation test, an optimum hardness of 461 HV was obtained. This result implies that the hardness test resulted in

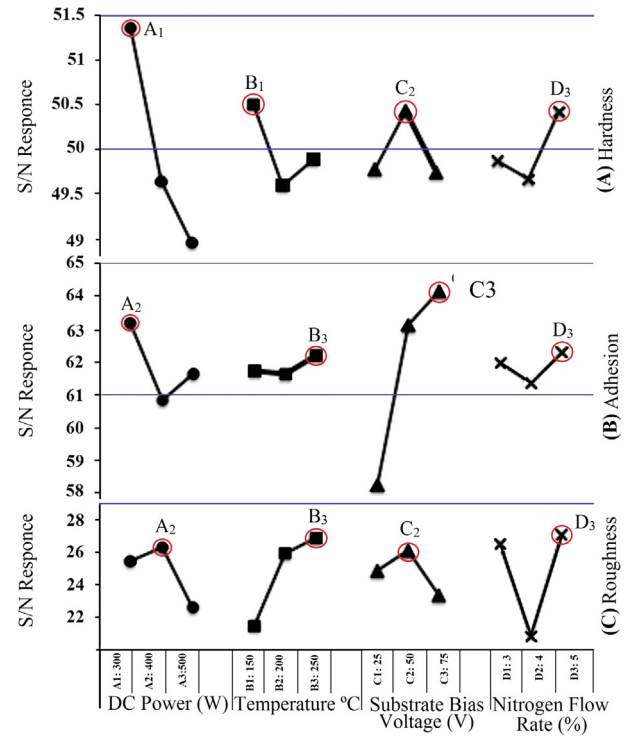


Fig. 7. The (S/N) response graph for surface (A) hardness, (B) scratch force, and (C) roughness.

Table 8
The (S/N) response values for surface roughness.

Symbol	Coating parameters	S/N response		
		Level 1	Level 2	Level 3
A	DC power (W)	25.47	26.29	22.58
B	Temperature (°C)	21.46	25.98	26.91
C	Substrate DC bias voltage (V)	24.93	26.10	23.32
D	Nitrogen flow rate (%)	26.50	20.80	27.05

Table 6
The (S/N) response values for surface hardness.

Symbol	Coating parameters	S/N response		
		Level 1	Level 2	Level 3
A	DC power (W)	51.37	49.64	48.95
B	Temperature (°C)	50.50	49.59	49.88
C	Substrate DC bias voltage (V)	49.78	50.43	49.75
D	Nitrogen flow rate (%)	49.86	49.67	50.42

Table 7
The (S/N) response values for scratch force.

Symbol	Coating parameters	S/N response		
		Level 1	Level 2	Level 3
A	DC power (W)	63.16	60.81	61.61
B	Temperature (°C)	61.74	61.62	62.21
C	Substrate DC bias voltage (V)	58.27	63.14	64.16
D	Nitrogen flow rate (%)	61.97	61.34	62.26

an improvement of 12% compared to the highest value of surface hardness achieved during the experiments, as shown in Table 5, and which corresponds to an improvement of 48% compared to the uncoated sample, which has a hardness of 312 HV. According to Fig. 7(B), the optimum combination to achieve the best adhesion was $A_1B_3C_3D_3$ where, based on the measured value of the scratch force S/N response, the adhesion of the confirmation test was 2207 mN, which represents an improvement of 5.1% compared to the best adhesion achieved during the experiments. Moreover, the results of the scratch test by means of measuring the friction load shown in Fig. 6 (graph c) reveal a coefficient of friction of 0.17. This is an improvement of 34% compared to a value of 0.26, which is for the best adhesion achieved during the experiments. Meanwhile, Fig. 7(C) illustrates the optimal combination for the surface roughness, which is $A_2B_3C_2D_3$. The surface roughness measured from the confirmation test was 0.0313 μm , which is a 10.52% improvement compared to the best surface roughness listed in Table 5.

The sputtering pressure of the chamber is related to the sputtering power. For a high chamber pressure, a low sputtering power results in a reduction of energy of sputtered atoms and this covers the substrate with charged particles [28]. At a constant pressure, the ion density is enhanced as a result of increasing the sputtering power. However, further increasing the power leads to a decrease of the sputtering rate because of back diffusion. In the current experiments, by increasing the DC power from 300 and 400 W, the sputtered and ionized particles became more energetic and therefore, the sputtering rate increased. A further increase of the DC power to 500 W results in increasing the collisions of sputtered particles with chamber particles (argon gas and ions). Hence, this increase of collisions leads to a dramatic fall of the sputtering rate for high power sputtering.

The effect of temperature is more critical in the surface hardness results. The result of the hardness test shows that the surface hardness of the coated substrate decreased when increasing the temperature from 150 to 250 °C. This may be the result of the slow movement of atoms at a low temperature. Increasing the temperature caused the atoms to move faster, which leads to a dense surface texture.

The DC bias voltage has a critical effect on the hardness of the TiN coating. By increasing the substrate bias voltage from 25 to 50 V, the hardness of the coated samples increased but the trend reversed when the voltage was increased from 50 to 75 V, as revealed in Fig. 8. Thus, uniformity of the TiN coating was improved with substrate biasing up to an optimal value and re-nucleation was observed to start above a critical bias value. Additionally, it is believed that the substrate temperature controls the diffusion of atoms during the TiN growth [47]. This affects the best condition for the surface hardness, which was obtained at a maximum temperature (i.e. B3) of 250 °C.

The mechanical properties of the TiN coating on Ti–6Al–4V were investigated at different conditions for the best adhesion, which resulted from the combination of $A_1B_3C_3D_3$, as shown in Fig. 7(B). It can be clearly observed that by increasing the DC bias voltage, the adhesion strength significantly improved. This can be ascribed to the additional energy available during the growth of the film. In other words, high-energy atoms have better mobility for finding the low energy sites on the surface to maximize the adhesion characteristics.

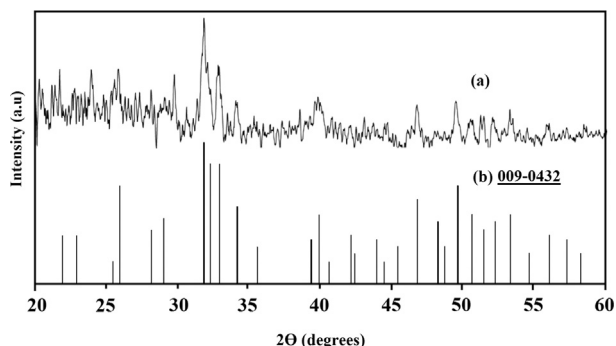


Fig. 8. (a) XRD pattern of HA layer coated on TiN layer, (b) relative chemical prescription for hydroxyapatite.

The best surface roughness was obtained for the combination of $A_2B_3C_2D_3$. Increasing the substrate DC bias voltage results in the coating surface phenomena. The surface roughness decreased with an increase of the substrate bias voltage from 25 to 50 V although it increased from 50 to 75 V, as shown in Fig. 7(C).

Further investigation revealed that the maximum adhesion strength of 2207 mN was achieved at a DC bias voltage of 75 V (C3). However, further increase of the DC bias voltage led to mechanical degradation of the film. However, the change of the temperature range had no significant effect on the scratch force (adhesion) [48].

Another important parameter which affects the adhesion between the substrate and coating is the nitrogen flow rate. The observed improvement of the adhesion strength can be attributed to the increase of the nitrogen flow rate. The deposited titanium interlayer decomposes the native oxide film on the substrate surface by acting as an oxygen scavenger, hence improving the adhesion between the substrate and coating. The nitrogen gas does not significantly change the chemical nature of α -Ti because no TiN compound was formed and nitrogen was dissolved in the α -Ti lattice. It is thus expected that the Ti interlayer influenced by nitrogen gas also plays a similar role as an oxygen scavenger.

On the contrary, too soft of an interfacial layer such as a pure Ti interlayer will deform too easily and provides less support to the TiN coating. Nitrogen gas makes the Ti layer stronger to provide better support for the TiN layer and increase the adhesion strength. However, further increasing

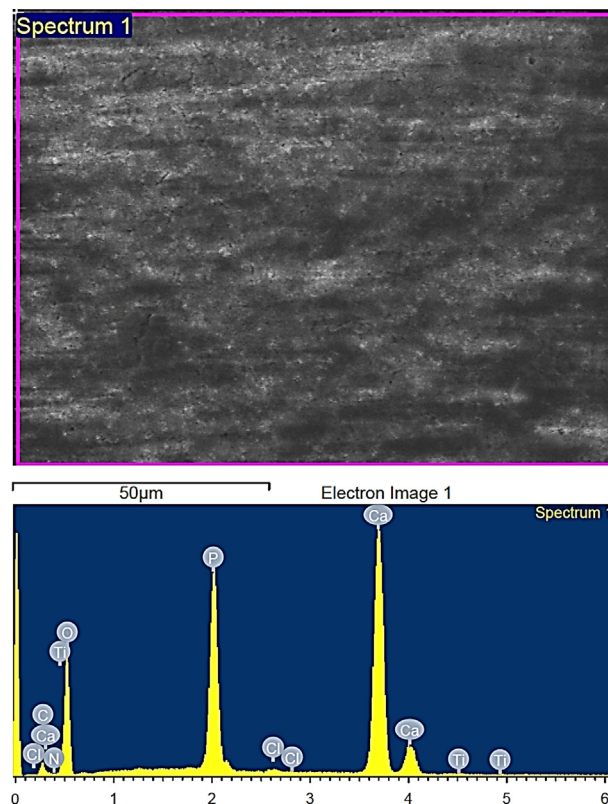


Fig. 9. EDX analysis of textured coating.

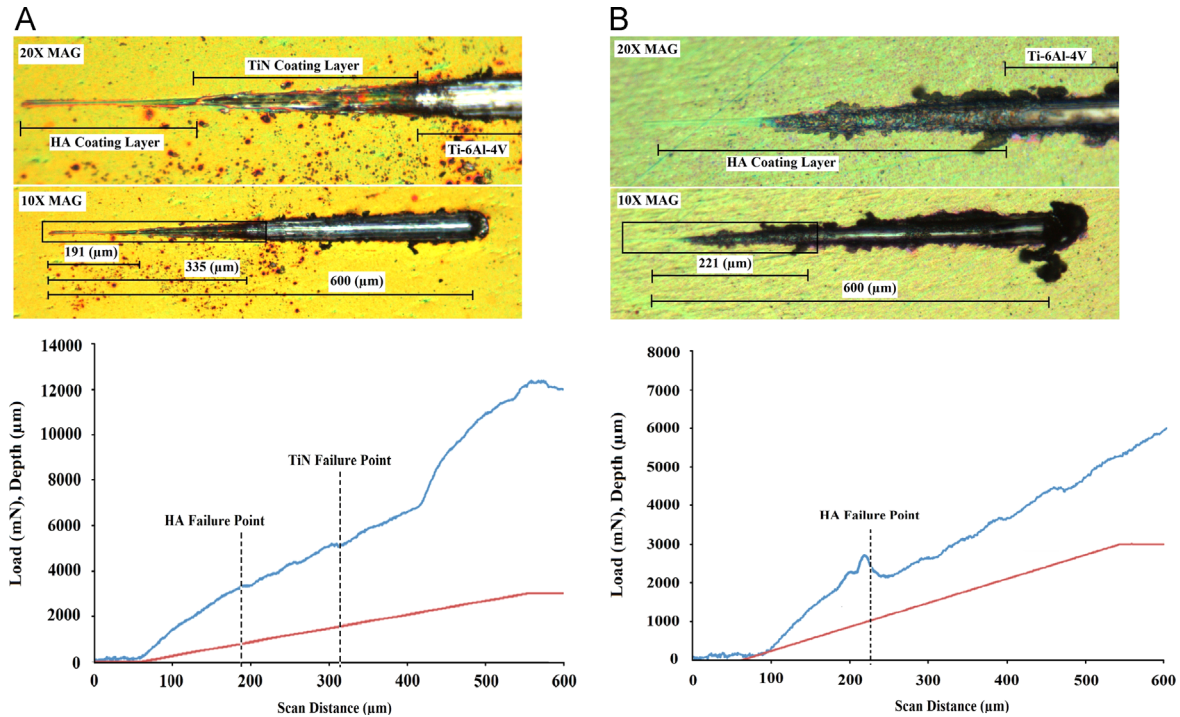


Fig.10. Scratch adhesion testing on a HA coated sample and the critical load accompany with their force and depth versus distance graphs. (A) HA/TiN coating Layer on Ti-6Al-4V, failure of HA and TiN are at 191 and 335 μm respectively. (B) HA coating Layer on Ti-6Al-4V, failure of HA is at 221 μm with corresponding load of 999.46 mN.

the amount of nitrogen resulted in a too strong and brittle of a surface to accommodate the interfacial stresses, which leads to a reduction of the adhesion strength. After the optimization, a nitrogen gas content of 4% seems to be a suitable amount to obtain the best adhesion strength.

4.5. Coating morphology and mechanical properties of the HA layer

Fig. 8 shows the X-ray diffraction patterns of hydroxyapatite. A HA thin film was subsequently deposited atop the Ti/TiN layer. The crystalline structure of the HA coating was investigated using X-ray diffraction (XRD) in the 2θ range from 20° to 60° . The figure shows that the XRD results of the HA-coated samples are in total agreement with the relative chemical prescription for hydroxyapatite (PDF. 009-0432). The presence of HA was also confirmed by energy dispersive X-ray (EDX) analysis (JEOL, JSM-760 F), as shown in Fig. 9.

Adhesion of the HA coating on the substrate was determined by the micro scratch test. The test was repeated three times in different places and the average value was calculated as the adhesion strength of the coated layer. Fig. 10(A) reports the results of microscratch test on the Ti/TiN/HA multi layers. The results show that HA was detached from the Ti/TiN surface at a distance of 191 μm with a corresponding load of 1445 mN. Meanwhile, the adhesion for the Ti/TiN layer after optimization was 2207 mN, which was attained at a scratch distance of 335 μm . Moreover, in another endeavor, a HA thin film was coated on Ti-6Al-4V under the same parameters to compare the adhesion strength of HA on the Ti/TiN layer and HA on the Ti-6Al-4V substrate. Fig. 10(B)

shows the microscratch test results for the HA coating layers formed by PVD on Ti-6Al-4V.

As reported above, the average adhesion strength in the case of Ti/TiN/HA was 1445 mN. On the other hand, a value of 999.46 mN was recorded with only the HA layer on the Ti alloy substrate. This result shows that by having a ceramic layer such as TiN layer as an interfacial layer between the HA thin film and substrate, the adhesion strength can increase by 44.57%.

5. Conclusions

In this study, the Taguchi optimization method was used with an orthogonal array of L_9 to achieve the optimal parameters for the best adhesion (scratch force), surface hardness, coefficient of friction, and surface roughness. Using the conceptual S/N ratio approach, the Taguchi's robust design was found to be a suitable method to analyze the TiN coating surface integrity using a magnetron sputtering technique on Ti-6Al-4V. The quantitative investigation suggested that a DC power of 300 W, temperature of 250°C , DC bias voltage of 75 V, and nitrogen flow rate of 5% resulted in the best adhesion of the coating to the substrate for the specific test range (TiN). Improved surface hardness was achieved with a DC power of 300 W, temperature of 150°C , substrate DC bias voltage of 50 V, and nitrogen flow rate of 5%. Furthermore, to achieve improved surface roughness, a DC power of 400 W, temperature of 250°C , DC bias voltage of 50 V, and nitrogen flow rate of 5% are suggested. The hardness of the TiN-coated Ti-6Al-4V samples increased up to 461 HV, while the hardness of the uncoated samples was 312 HV. The

confirmation tests demonstrated improvements of 5.1%, 43%, and 10.52% for the adhesion, coefficient of friction, and surface roughness, respectively. The test also demonstrates that the surface hardness values of the coated and uncoated samples were enhanced to 14% and 48%, respectively. Hydroxyapatite was successfully deposited on the optimized Ti/TiN coating. The HA thin film shows a similar chemical composition, as reported by other researchers. The results also demonstrate that applying a Ti/TiN thin film as an interfacial layer may improve the adhesion of the HA coating on Ti–6Al–4V by 44.57%.

Acknowledgments

This research was funded by a Hanyang University's Research Fund (201500000000438), Ministry of Higher Education, Malaysia along with a high impact research Grant (UM.C/625/1/HIR/MOHE/ENG/27) and a Human Resources Program in Energy Technology of the Korea Institute of Energy Technology Evaluation and Planning (KETEP) Grant from the Ministry of Trade, Industry and Energy, Republic of Korea (No. 20154030200900).

References

- [1] M. Sarrafa, E. Zalnezhad, A.R. Bushroa, A.M.S. Hamouda, A.R. Rafieerad, B. Nasiri-Tabrizi, Effect of microstructural evolution on wettability and tribological behavior of TiO₂ nanotubular arrays coated on Ti–6Al–4V, *Ceram. Int.* 41 (2015) 7952–7962.
- [2] R.S. Namba, J.H. Keyak, A.S. Kim, L.P. Vu, H.B. Skinner, Cementless implant composition and femoral stress: a finite element analysis, *Clin. Orthop. Relat. Res.* 347 (1998) 261.
- [3] J.J. Jacobs, J.L. Gilbert, R.M. Urban, Current concepts review-corrosion of metal orthopaedic implants, *J. Bone Jt. Surg. (Am.)* 80 (1998) 268–282.
- [4] J.O. Galante, J. Lemons, M. Spector, P.D. Wilson Jr, T.M. Wright, The biologic effects of implant materials, *J. Orthop. Res.* 9 (1991) 760–775.
- [5] U. Bischoff, M. Freeman, D. Smith, M. Tuke, P. Gregson, Wear induced by motion between bone and titanium or cobalt-chrome alloys, *J. Bone Jt. Surg. Br.* 76 (1994) 713–716.
- [6] K. Hirakawa, B.N. Stulberg, A.H. Wilde, T.W. Bauer, M. Secic, Results of 2-stage reimplantation for infected total knee arthroplasty, *J. Arthroplast.* 13 (1998) 22–28.
- [7] H. McKellop, A. Sarmiento, C.P. Schwin, E. Ebrahmdadeh, In vivo wear of titanium-alloy hip prostheses, *J. Bone Jt. Surg. Am.* 72 (1990) 512.
- [8] C. Peterson, B. Hillberry, D. Heck, Component wear of total knee prostheses using Ti–6Al–4V, TiN coated Ti–6Al–4V, and Co–Cr–Mo femoral components, *J. Biomed. Mater. Res.* 22 (1988) 887–903.
- [9] W.W. Brien, E.A. Salvati, F. Betts, P. Bullough, T. Wright, C. Rimnac, R. Buly, K. Garvin, Metal levels in cemented total hip arthroplasty: a comparison of well-fixed and loose implants, *Clin. Orthop. Relat. Res.* 276 (1992) 66–74.
- [10] E.A. Salvati, F. Betts, S.B. Doty, Particulate metallic debris in cemented total hip arthroplasty, *Clin. Orthop. Relat. Res.* 293 (1993) 160–173.
- [11] H.W. Jang, H.-J. Lee, J.-Y. Ha, K.-H. Kim, T.-Y. Kwon, Surface characteristics and osteoblast cell response on TiN- and TiAlN-coated Ti implant, *Biomed. Eng. Lett.* 1 (2011) 99–107.
- [12] A.V. Lombardi Jr, T. Mallory, B. Vaughn, P. Drouillard, Aseptic loosening in total hip arthroplasty secondary to osteolysis induced by wear debris from titanium-alloy modular femoral heads, *J. Bone Jt. Surg. Am.* 71 (1989) 1337–1342.
- [13] J.M. Cuckler, J. Bearcroft, C.M. Asgarian, Femoral head technologies to reduce polyethylene wear in total hip arthroplasty, *Clin. Orthop. Relat. Res.* 317 (1995) 57–63.
- [14] B. Coll, M. Pellman, Metallurgical and tribological modifications of titanium and titanium alloys by plasma assisted techniques, in: *Proceedings of the Society for Biomaterials Implant Retrieval Symposium*, 1992.
- [15] J. Kawalec, S. Brown, Fretting corrosion of untreated and nitrided Ti6Al4V fretted against bone and bone cement, *Trans. Soc. Biomater.* 18 (1995) 355.
- [16] F.F. Buechel, M.J. Pappas, G. Makris, Evaluation of contact stress in metal-backed patellar replacements, *Clin. Orthop. Relat. Res.* 273 (1991) 190–197.
- [17] M.K. Harman, S.A. Banks, W.A. Hodge, Polyethylene damage and knee kinematics after total knee arthroplasty, *Clin. Orthop. Relat. Res.* 392 (2001) 383–393.
- [18] J. Li, H. Liao, B. Normand, C. Cordier, G. Maurin, J. Foct, C. Coddet, Uniform design method for optimization of process parameters of plasma sprayed TiN coatings, *Surf. Coat. Technol.* 176 (2003) 1–13.
- [19] S. Logothetidis, I. Alexandrou, S. Kokkou, Optimization of TiN thin film growth with in situ monitoring: the effect of bias voltage and nitrogen flow rate, *Surf. Coat. Technol.* 80 (1996) 66–71.
- [20] M. Farooq, Z. Lee, Optimization of the sputtering process for depositing composite thin films, *J. Korean Phys. Soc.* 40 (2002) 511–515.
- [21] P. Mayrhofer, C. Mitterer, J. Musil, Structure–property relationships in single- and dual-phase nanocrystalline hard coatings, *Surf. Coat. Technol.* 174 (2003) 725–731.
- [22] B. Arzamasov, S. Babich, L. Kirichenko, V. Knyazheva, V. Silaeva, T. Solov'eva, Properties of aluminum alloys with a titanium nitride coating, *Met. Sci. Heat Treat.* 36 (1994) 308–312.
- [23] G. Majzoubi, M. Jaleh, Duplex surface treatments on AL7075-T6 alloy against fretting fatigue behavior by application of titanium coating plus nitriding, *Mater. Sci. Eng. A* 452 (2007) 673–681.
- [24] I. Efeoglu, A. Celik, Mechanical and structural properties of AISI 8620 steel TiN coated, nitrided and TiN coated + nitrided, *Mater. Charact.* 46 (2001) 311–316.
- [25] E. Mohseni, E. Zalnezhad, A. Bushroa, Comparative investigation on the adhesion of hydroxyapatite coating on Ti–6Al–4V implant: a review paper, *Int. J. Adhes. Adhes.* 48 (2014) 238–257.
- [26] H. Aoki, Science and Medical Applications of Hydroxyapatite, Ishiyaku Euroamerica, 1991.
- [27] B. Subramanian, M. Jayachandran, Characterization of reactive magnetron sputtered nanocrystalline titanium nitride (TiN) thin films with brush plated Ni interlayer, *J. Appl. Electrochem.* 37 (2007) 1069–1075.
- [28] C.W. Tan, J. Miao, Optimization of sputtered Cr/Au thin film for diaphragm-based MEMS applications, *Thin Solid Films* 517 (2009) 4921–4925.
- [29] J.-H. Huang, K.-W. Lau, G.-P. Yu, Effect of nitrogen flow rate on structure and properties of nanocrystalline TiN thin films produced by unbalanced magnetron sputtering, *Surf. Coat. Technol.* 191 (2005) 17–24.
- [30] Eleonora Santeccchia, A.M.S. Hamouda, Farayi Musharavati, Erfan Zalnezhad, Marcello Cabibbo, Stefano Spigarelli, Wear resistance investigation of titanium nitride-based coatings, *Ceram. Int.* 41 (2015) 10349–10379.
- [31] P. Mayrhofer, F. Kunc, J. Musil, C. Mitterer, A comparative study on reactive and non-reactive unbalanced magnetron sputter deposition of TiN coatings, *Thin Solid Films* 415 (2002) 151–159.
- [32] M. Diesselberg, H. Stock, P. Mayr, Corrosion protection of magnetron sputtered TiN coatings deposited on high strength aluminium alloys, *Surf. Coat. Technol.* 177 (2004) 399–403.
- [33] R.K. Roy, Design of Experiments Using the Taguchi Approach: 16 Steps to Product and Process Improvement, Wiley.com, 2001.
- [34] E. Zalnezhad, A.A.D.M. Sarhan, M. Hamdi, Prediction of TiN coating adhesion strength on aerospace AL7075-T6 alloy using fuzzy rule based system, *Int. J. Precis. Eng. Manuf.* 13 (2012) 1453–1459.
- [35] M.A. Ezazi, M.M. Quazi, E. Zalnezhad, A.A.D. Sarhan, Enhancing the tribo-mechanical properties of aerospace AL7075-T6 by magnetron-sputtered Ti/TiN, Cr/CrN & TiCr/TiCrN thin film ceramic coatings, *Ceram. Int.* 40 (10) (2014) 15603–15615.
- [36] E. Zalnezhad, A.M.S. Hamouda, G. Faraji, S. Shamshirband, TiO₂ nanotube coating on stainless steel 304 for biomedical applications, *Ceram. Int.* 41 (2015) 2785–2793.
- [37] A. Mubarak, P. Akhter, E. Hamzah, M.R.H.M. Toff, I.Q.A. Qazi, Effect of coating thickness on the properties of tin coatings deposited on tool

- steels using cathodic arc PVD technique, *Surf. Re. Lett.* 15 (2008) 401–410.
- [38] J. Ghani, I. Choudhury, H. Hassan, Application of Taguchi method in the optimization of end milling parameters, *J. Mater. Process. Technol.* 145 (2004) 84–92.
- [39] I. Asiltürk, H. Akkuş, Determining the effect of cutting parameters on surface roughness in hard turning using the Taguchi method, *Measurement* 44 (2011) 1697–1704.
- [40] H.S. Kim, A combined FEA and design of experiments approach for the design and analysis of warm forming of aluminum sheet alloys, *Int. J. Adv. Manuf. Technol.* 51 (2010) 1–14.
- [41] R. Shetty, R.B. Pai, S.S. Rao, R. Nayak, Taguchi's technique in machining of metal matrix composites, *J. Braz. Soc. Mech. Sci. Eng.* 31 (2009) 12–20.
- [42] E. Zalnezhad, A.A. Sarhan, M. Hamdi, Optimizing the PVD TiN thin film coating's parameters on aerospace AL7075-T6 alloy for higher coating hardness and adhesion with better tribological properties of the coating surface, *Int. J. Adv. Manuf. Technol.* 64 (2013) 281–290.
- [43] L. Dobrzański, M. Polok, M. Adamiak, Structure and properties of wear resistance PVD coatings deposited onto X37CrMoV5-1 type hot work steel, *J. Mater. Process. Technol.* 164 (2005) 843–849.
- [44] B. Beake, A. Ogwu, T. Wagner, Influence of experimental factors and film thickness on the measured critical load in the nanoscratch test, *Mater. Sci. Eng. A* 423 (2006) 70–73.
- [45] W. Brostow, J.-L. Deborde, M. Jaclewicz, P. Olszynski, Tribology with emphasis on polymers: friction, scratch resistance and wear, *J. Mater. Educ.* 25 (2003) 119–132.
- [46] G. Amontons, De la resistance causee dans les machines, *Mem. de l'Academie Royal A*, pp. 275–282.
- [47] K.-L. Choy, E. Felix, Functionally graded diamond-like carbon coatings on metallic substrates, *Mater. Sci. Eng. A* 278 (2000) 162–169.
- [48] Y. Chunyan, T. Linhai, W. Yinghui, W. Shebin, L. Tianbao, X. Bingshe, The effect of substrate bias voltages on impact resistance of CrAlN coatings deposited by modified ion beam enhanced magnetron sputtering, *Appl. Surf. Sci.* 255 (2009) 4033–4038.